China Geology 7 (2024) 291−302

China Geology

Journal homepage: http://chinageology.cgs.cn
https://www.sciencedirect.com/journal/china-geology

Unraveling the hydraulic properties of loess for landslide prediction: A study on variations in loess landslides in Lanzhou, Dingxi, and Tianshui, China

Gao-chao Lin[a], Wei Liu[b,*], Xing Su[c]

[a] *School of Civil and Environmental Engineering, University of New South Wales, Sydney, NSW* 2052, *Australia*
[b] *Institute of Transportation, Inner Mongolia University, Hohhot* 010070, *China*
[c] *Institute of Geological Hazards Prevention, Gansu Academy of Sciences, Lanzhou* 730000, *China*

ARTICLE INFO

Article history:
Received 9 January 2024
Received in revised form 4 April 2024
Accepted 6 April 2024
Available online 18 April 2024

Keywords:
Loess
Landslide
Hydraulic properties
Water retention capacity and permeability
Soil Water Characteristic Curve (SWCC)
Hydraulic conductivity
Van Genuchten model
Hydrogeological engineering
Geological hazards prevention engineering

ABSTRACT

Loess has distinctive characteristics, leading to frequent landslide disasters and posing serious threats to the lives and properties of local residents. The involvement of water represents a critical factor in inducing loess landslides. This study focuses on three neighboring cities sequentially situated on the Loess Plateau along the direction of aeolian deposition of loess, namely Lanzhou, Dingxi, and Tianshui, which are densely populated and prone to landslide disasters. The variations in hydraulic properties, including water retention capacity and permeability, are investigated through Soil Water Characteristic Curve (SWCC) test and hydraulic conductivity test. The experimental findings revealed that Tianshui loess exhibited the highest water retention capacity, followed by Dingxi loess, while Lanzhou loess demonstrated the lowest water retention capacity. Contrastingly, the results for the saturated permeability coefficient were found to be the opposite: Tianshui loess showed the lowest permeability, whereas Lanzhou loess displayed the highest permeability. These results are supported and analyzed by scanning electron microscopy (SEM) observation. In addition, the water retention capacity is mathematically expressed using the van Genuchten model and extended to predict unsaturated hydraulic properties of loess. The experimental results exhibit a strong accordance with one another and align with the regional distribution patterns of disasters.

1. Introduction

Loess, a distinct Quaternary geological formation, displays a broad distribution worldwide, spanning across multiple continents including Asia, Europe, and North and South America (Taylor SR et al., 1983; Metelková Z et al., 2012; Lin GC et al., 2023). It is noteworthy that China alone possesses a considerable expanse of approximately 631000 km^2 of loess, which corresponds to roughly 6.6% of the nation's total land area. The most significant accumulation of these deposits covers an area of approximately 317000 km^2, and forms the famous Loess Plateau, which is the largest and most notable formation of its kind on Earth (Liu TS et al., 1964; Liu TS, 1985; Derbyshire E, 2000, 2001).

The Loess Plateau exhibits an arid and semi-arid climate that is influenced by the Asian monsoon and its fluctuations. During the winter season, the region primarily experiences cold and dry winds due to the influence of the Mongolian-Siberian high-pressure system. Conversely, in summer, the breakdown of the Mongolian-Siberian high-pressure system leads to the influx of warm and moist oceanic air from the Indian Ocean and South China Sea. This change in weather patterns brings about intense and prolonged rainfall, predominantly occurring in the months of July, August, and September.

Additionally, it is important to note that aeolian deposits exhibit a fundamental characteristic whereby the particle size of deposited materials gradually decreases in the direction of wind transport. This pattern is evident in arid and semi-arid zones at mid-latitudes, where gobi, desert, and loess are sequentially distributed along the developmental path of aeolian deposits. Therefore, the properties of loess, represented by particle size, should gradually change in the direction of aeolian deposition on a macroscopic level. In

First author: *E-mail address*: gaochao.lin@unsw.edu.au (Gao-chao Lin).
* Corresponding author: *E-mail address*: liuwei@imu.edu.cn (Wei Liu).

Literary editor: Li-qiong Jia
doi:10.31035/cg2024006
2096-5192/© 2024 China Geology Editorial Office.

other words, changes in loess properties follow a certain regularity at the regional level.

Loess is characterized by its uniform texture and developed porosity. When the moisture content is low, the clay particles in loess can exhibit high matric suction within the soil structure, thereby agglomerating around coarser grains and playing a supporting role. Additionally, the secondary calcium carbonate present in loess acts as a cementing agent. These combined phenomena contribute to the increased strength of loess under low moisture conditions. However, this characteristic also leads to certain vulnerabilities when the soil comes into contact with water, such as heavy rainfall or irrigation. The surface tension between clay particles is released, causing the fine particles to become loose and wash out. Meanwhile, the crystallized salts dissolve during this process, thereby eliminating the cementation effect. Consequently, due to the release of matric suction and dissolution of salts, loess instantaneously disintegrates under its own weight, which is referred to as collapsibility (Derbyshire E, 2001; Wu WJ, 2003; Cheng YX et al., 2007; Xin CL et al., 2012; Guo FY et al., 2015). The unique structural properties of loess contribute to its vulnerability to rain-induced erosion during rainy season. Moreover, the growing urban population and subsequent increase in agricultural demand have resulted in larger-scale and more extensive irrigation practices, thereby exposing the loess to higher risks associated with water exposure. Additionally, the frequent occurrence of seismic stress and erosion-induced unloading further facilitate the development of vertical joints within loess deposits. These vertical joint systems, in turn, give rise to the formation of sub-horizontal joints, leading to the creation of intricate drainage networks, exacerbating the degradation of loess.

Compounding the issue is the fact that in the Loess Plateau region, loess is predominantly deposited on Cretaceous to Neogene mudstone. Mudstone, due to its extremely low permeability coefficient, is commonly considered as a water-resistant layer in the formation. Consequently, water that infiltrates the upper layer of loess and reaches the top surface of the mudstone is unable to dissipate promptly, leading to accumulation. As a result, the moisture content in the loess near the contact surface is elevated, and in extreme cases, it becomes saturated. Previous studies by Derbyshire E (2000, 2001), Wen BP et al. (2012), Xu L et al. (2018), Liang CY et al. (2022), and Zhang ZL et al. (2022,2023), to name a few, have all substantiated these findings.

In summary, the frequent occurrence of landslide disasters in the Loess Plateau can be attributed to several factors, including the inherent structural characteristics of loess, the stratigraphic distribution of the area, the intensified seismic activity resulting from the tectonic movement of the Himalayan-Tibetan Plateau, the concentrated rainfall patterns brought about by the monsoon climate, and the increased irrigation water due to the ongoing urbanization development. Collectively, these factors contribute to the high vulnerability of the region to landslide occurrences, posing a serious threat to the lives and properties of the local population.

Scholars have conducted extensive geological survey on landslides occurring in loess areas, and classified them based on stratigraphic occurrence and distribution of loess and mudstone, as well as the characteristics of landslides. For example, Wu WJ et al. (2002) categorized loess landslides into four types according to the material composition of the landslides and their activity characteristics, including loess landslides, loess-mudstone interface landslides, loess-mudstone bedding landslides, and loess-mudstone incision landslides. Li TL et al. (2007) classified loess landslides into four types based on their movement modes: Staggered landslides, high-speed remote landslides, low-speed slow-moving landslides, and landslide mudflows. Further research on landslide classification can be found in the work of Wu WJ et al. (2008), Xu L et al. (2008, 2010), Li YR and Mo P (2019), and others.

The studies in the existing literature about loess landslides have primarily focused on examining the distinct behaviors of loess and mudstone in response to dynamic loading from different aspects. For instance, Zhang ZL et al. (2017) conducted centrifuge shaking table tests and numerical simulations to investigate the dynamic behavior of loess and mudstone. They explored the effects of height, lithology, and surface conditions on Peak Ground Acceleration (PGA) amplification factors and determined the corresponding displacements of loess and mudstone. Chen JC et al. (2022) investigated the failure mechanism of loess-mudstone landslides and found that the energy response differed significantly between the two media. Other researchers, including Lin ML and Wang KL (2006), Wang KL and Lin ML (2011), Srilatha N et al. (2013), Huang QB et al. (2019), Jia XN et al. (2022), Yu TF et al. (2023), and Liu W et al. (2023) among many others, have made similar attempts to study these phenomena. Another major research area in the literature focuses on the mechanical properties of loess and mudstone under various conditions. Zhang S et al. (2016) examined the effects of rainwater softening on mudstone through laboratory tests, and they observed a reduction in the shear strength of mudstone when subjected to rainwater infiltration, which they attributed to structural changes in clay minerals. Wang XG et al. (2021) employed ring shear tests and numerical simulations to study the triggering mechanism of loess landslides and they found that both peak strength and residual strength decreased with increasing moisture content.

Regarding the hydraulic properties of loess, the research primarily focuses on examining the physical characteristics of the loess, such as permeability (Wang H et al., 2014; Hu HJ, 2018), and investigating the infiltration characteristics of water in loess (Liu FY and Zhang Z, 2008; Zhang CL et al., 2014) as well as the resulting erosion (Walder JS, 2016; Khanal A, 2016). However, there is relatively less research focusing on the water retention capacity of loess and even fewer studies that directly associates these properties with landslide stability. The existing studies related to the water

holding capacity of loess mainly focus on the fields of plantation or irrigation practice (Jiao X et al., 2014; Wang X et al., 2015). However, as previously mentioned, the presence of mudstone in the loess leads to the enrichment and retention of water. Consequently, the water retention capacity of the loess plays a vital role in determining the overall stability of the slope. The water retention capacity of loess can be described by the Soil Water Characteristic Curve (SWCC), also known as the Soil Water Retention Curve (SWRC). This curve is typically presented as a graph showing the logarithm of either matric suction or total suction against either the degree of saturation, gravimetric water content, or volumetric water content. Additionally, the SWCC plays a crucial role in accurately characterizing the properties of unsaturated soil, such as its strength, permeability, and volume change. Understanding these aspects is essential in assessing the stability of landslides. Hence, gaining a thorough understanding of the SWCC in soils associated with loess landslides provides comprehensive insights into the inherent nature of landslides and their development patterns.

Based on these considerations, this study explores the relationship between changes in the hydraulic properties of loess in macro-regional areas and the occurrence of loess mudstone landslide disasters in these regions. To achieve this, three neighboring cities characterized with frequent occurrence of loess landslides, namely Lanzhou, Dingxi, and Tianshui, were selected sequentially along the development direction of the Loess Plateau to conduct research (Xin ZX and Han QX, 1988; Wang SQ and Unwin DJ, 1992; Xu YR et al., 2020). Moreover, comprehensive field sampling, indoor experimental research, and subsequent theoretical analysis were conducted to fulfill the investigation on the correlation between the hydraulic properties of loess and landslide hazards.

2. Loess landslide case study

This research focuses on three loess landslides that have either recently occurred or are presently ongoing in the landslide-prone regions of Lanzhou City, Dingxi City, and Tianshui City, which are sequentially located on Loess Plateau along the direction of aeolian deposition of loess. The three landslides chosen for study have undergone geological surveys and investigations conducted by other researchers, and are considered to be fairly representative of loess landslides in the region. These three adjacent cities share similar geological characteristics, including comparable tectonic movement, stratigraphic distributions, and climatic conditions. Owing to the densely populated nature of the area and the rapid pace of urbanization, landslides transpire with increased frequency, resulting in far-reaching consequences. The following Fig. 1 depicts the recorded distribution of landslides in this specific region, as documented in literature. It illustrates the elevated occurrence of landslide hazards surrounding these three cities, underscoring the significance of investigating the hazards associated with loess landslides.

2.1. Jiuzhou landslide in Lanzhou

The landslide is situated within the Jiuzhou economic development zone, specifically in Lanzhou City. The image of Jiuzhou landslide is shown in Fig. 2. The upper portion of the slope is comprised of a layer of Malan loess, characterized by a gradient ranging from 20° to 30°. Transitioning to the lower part, Gaolan Group mudstone is present, exhibiting a steep inclination of 40° to 50°. Notably, during the construction of Jiuzhou Avenue, the front section of the slope was aligned with the roadworks. As a result, partial slope cutting and slope toe excavation were conducted, pushing the hillside approximately 10 m backward and intensifying the slope angle.

The Jiuzhou landslide exhibits a length of 75 m, with a trailing edge width measuring 25 m and a front edge width of 95 m. The total area affected by the landslide spans approximately 4050 m^2. Within the landslide body, the maximum thickness at the central region reaches 17.6 m,

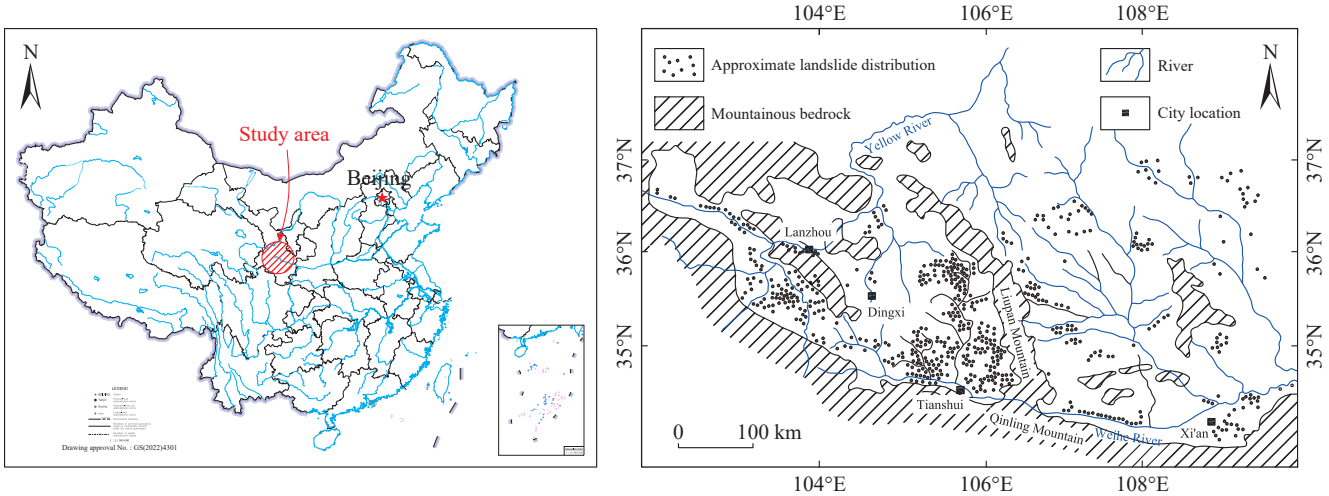

Fig. 1. Schematic of landslide distribution and basic landform conditions near Lanzhou, Dingxi and Tianshui on the Loess Plateau (Fig. b after Derbyshire E, 2001) .

while the average thickness is estimated to be around 13 m. The volume of the landslide remaining on the slide bed is about 5.4×10^4 m^3, and there is an additional sliding body of approximately 0.8×10^4 m^3 that has fallen, resulting a total volume of about 6.2×10^4 m^3. The primary sliding direction is oriented at an angle of 55° (Mu P et al., 2010).

The formation mechanism of the landslide can be attributed to the prolonged action of its own weight and the influence of precipitation, resulting in gradual creeping deformation of the landslide body, ultimately leading to complete destruction. The mountainous topography within the landslide area is characterized by significant height and steepness, which facilitates the accumulation of potential energy, thereby contributing to the development and formation of landslides. Moreover, the upper portion of the slope comprises loose loess structure, characterized by the presence of vertical joints and sinkholes, which provides favorable conditions for rainwater infiltration. During the rainy season, the influx of rainwater increases the weight of the landslide and deteriorates the properties of the loess. Additionally, human-engineered activities constitute another significant contributing factor to the occurrence of this landslide.

2.2. Huanancun landslide in Tianshui

The Huanancun landslide derives its name from its location in Huanancun Village, Maiji District, Tianshui City. The photo of Huanancun landslide is presented in Fig. 3. The sliding bed of the Huanancun landslide primarily consists of Neogene mudstone. The mudstone layers are typically characterized by considerable thickness and relatively undeveloped bedding planes. With the exception of the basin periphery and the proximity to the fault zone, the rock formations generally demonstrate nearly horizontal orientation. The mudstone layer is primarily overlain by Malan loess, which represents a light grayish-yellow soil exhibiting a uniform texture and well-developed porosity.

The landslide spans a total length of 95 m and has a width of 130 m. Its thickness ranges between 5–10 m, encompassing an area of 1.24×10^4 m^2 and a volume of approximately 1.24×10^5 m^3. The rear edge of the landslide is situated at an elevation of 1210 m, whereas the front edge rests at 1170 m,

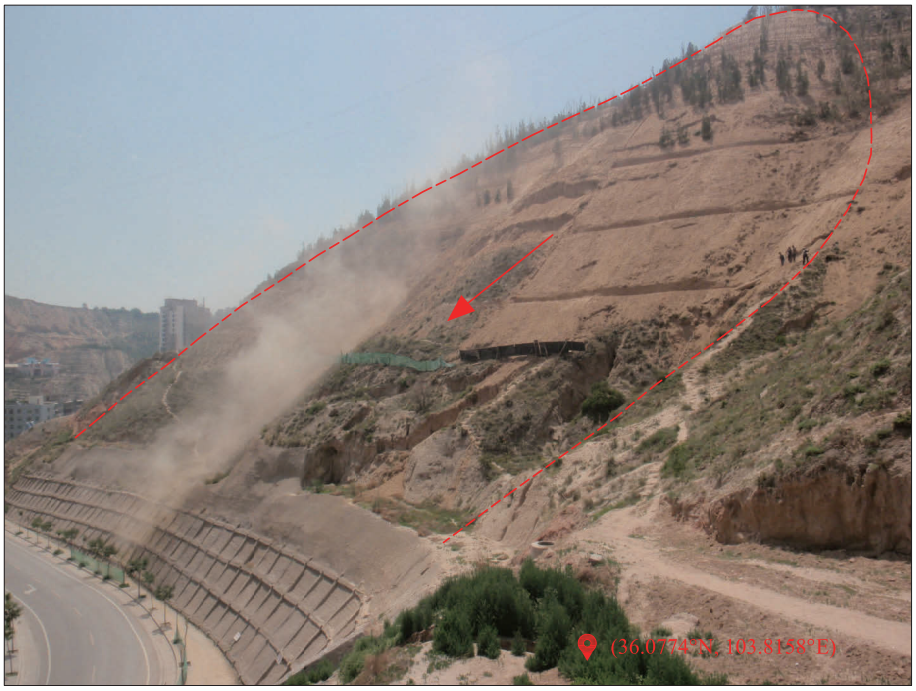

Fig. 2. Field photograph of Jiuzhou landslide in Lanzhou City.

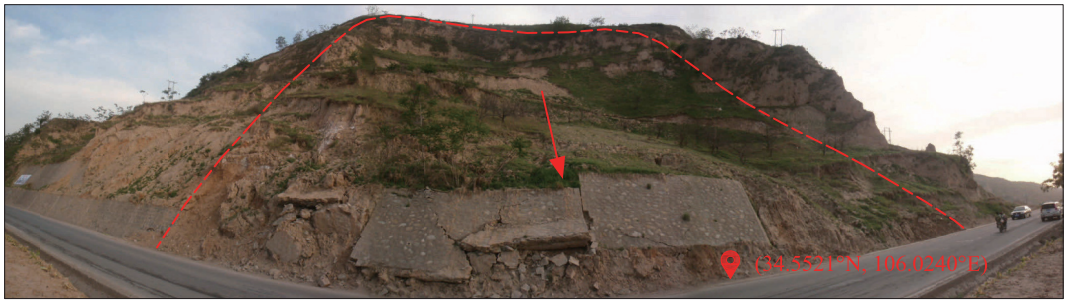

Fig. 3. Field photograph of Huanancun landslide in Tianshui City.

resulting in a significant 40 m difference in elevation. The surface of the landslide has an average slope of approximately 16° (Chen WW et al, 2016).

landslides primarily occur as a result of the moisture generated through the spring thaw, as well as spring plowing and irrigation practices, which causes the moisture accumulation on the top surface of mudstone. This moisture accumulation in loess leads to an increase in the weight of the landslide mass, and a reduction in the shear resistance of the loess in the sliding zone. As a result, these factors collectively trigger devastating landslide.

2.3. Changjiahe landslide in Dingxi

The Changjiahe landslide is situated in Changjiahe Town, Tongwei County, Dingxi City. The image of Changjiahe landslide is provided in Fig. 4. The study area primarily consists of Paleogene and Neogene mudstone, covered by Malan loess sediment. The landslide measures approximately 560 m in length and 800 m in width, with an average thickness of about 20 m and a volume of around 7.74×10^6 m^3. The highest elevation of the landslide reaches approximately 1620 m, while the sliding outlet at the riverbed sits at an elevation of about 1500 m. Thus, the height difference of the landslide amounts to 120 m, with a maximum sliding distance of approximately 60 m (Wang HJ et al. 2020).

The landslide body exhibits tensile cracks and shear cracks, varying in length from 10 m to 200 m and width from 0.2 m to 5.0 m. Following an extended period of gradual movement, the sliding body eventually reached the bottom of the Kushui River valley and was ultimately halted by the terraces in the opposite valley. As a result, the landslide accumulation effectively blocked the river channel for approximately 1 km.

The mechanism of landslide formation is that the Changjia River erodes downward to form a free surface, and the loess at the front edge of the slope creeps toward the free surface due to loss of confinement. Rainfall further exacerbates the movement, causing an increase in the self-weight of the landslide. This excess moisture also saturates the loess at the contact surface, thereby reducing its strength. Consequently, the landslide body undergoes reactivation in conjunction with the original historical earthquake-induced landslide.

3. Test material

The loess soils utilized in this study were extracted from the rear walls of the three aforementioned landslides by excavating pits to a certain depth and were taken from soils with uniform structure. This careful approach ensured the preservation of the loess structure and the representativeness of the samples, preventing disturbance caused by landslide events or the inclusion of extraneous debris due to landslides. For the sake of subsequent discussions, the loess samples obtained from Lanzhou, Tianshui, and Dingxi are respectively designated as LZ loess, TS loess, and DX loess.

After excavation, the soil samples were carefully placed in airtight containers and subsequently transported to the laboratory for testing. The undisturbed loess soil then underwent a series of fundamental geotechnical experiments to determine the essential characteristics, including the measurement of natural moisture content, density, specific gravity, plastic and liquid limits, as well as the analysis of particle size distribution (PSD). The experimental results are shown in the Table 1 below, and the PSD curves are presented in Fig. 5. It can be seen that the Tianshui loess exhibits a greater proportion of fine-grained components, followed by the Tongwei loess, while the Lanzhou loess displays the least amount.

Fig. 4. Field photograph of Changjiahe landslide in Dingxi City.

Table 1. Basic physical indices of loess.

Soil Sample	Water content/%	Bulk density/(g/cm^3)	Void ratio	Specific gravity	Plastic limit /%	Liquid limit /%	Plastic index
LZ Loess	7.31	1.51	0.92	2.70	18.66	28.72	10.06
TS Loess	8.03	1.56	0.88	2.72	19.04	29.50	10.46
DX Loess	7.62	1.53	0.89	2.69	21.23	31.40	10.17

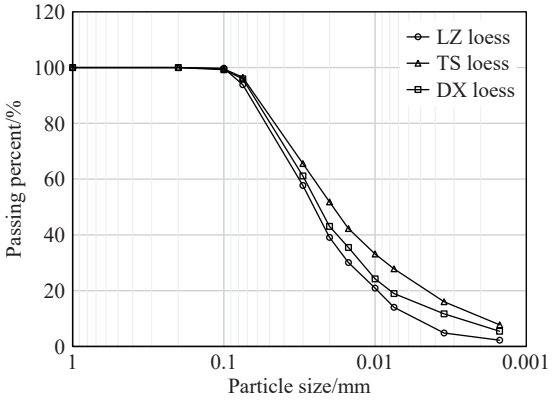

Fig. 5. Particle size distribution curves of LZ, TS and DX loess samples.

4. Methodology

The loess samples used for soil water characteristics curve experiments were obtained by carefully cutting undisturbed loess with a containing ring. The SWCC of the prepared samples were determined using the pressure plate method. This method involves the use of a porous ceramic plate with a high air entry value (AEV), which establishes a pressure gradient between the pore water pressure (u_w) within the plate and the externally applied air pressure (u_a). In the experiment, saturated soil samples are placed on the porous plate inside a sealed chamber, initiating the drainage of pore fluid from the soil samples through the plate due to the established pressure difference. Once equilibrium is reached, the soil samples resting on the plate exhibit a matric suction, which corresponds to the pressure difference between the applied u_a and u_w. Subsequently, the water content of the samples is determined. To construct the soil water characteristic curve, this procedure is iteratively conducted with various air pressures. By measuring the water content at each pressure level, a plot representing the behavior of water within the soil can be obtained. It should be noted that achieving equilibrium for each pressure level requires a minimum duration of one week. Therefore, to obtain a comprehensive soil water characteristic curve encompassing an air pressure range from 0 kPa to 1500 kPa, approximately two months are typically required. Despite its lengthy and time-consuming nature, the pressure plate method offers several advantages over other methods. It allows for direct and reliable control over the matric suction within the soil samples, enhancing the accuracy of the obtained data. Fig. 6 presents a typical schematic of the pressure plate equipment used in this method.

After collecting the pressure plate data, they are then subjected to simulation and analysis. In the field of geotechnical and geological engineering, various formulas have been proposed to mathematically represent the soil water characteristic curve (SWCC). Among the most widely recognized models are the Brooks and Corey model (Brooks R and Corey A, 1964), van Genuchten model (van Genuchten MT, 1980), and Fredlund and Xing model (Fredlund DG and Xing A, 1994). To simplify, these models are referred to as the BC model, VG model, and FX model, respectively. The BC model, being one of the earliest and simplest equations for SWCC, is suitable for coarse-grained soils within relatively low suction ranges. On the other hand, the VG model incorporates a strong physical and theoretical foundation by considering the soil's pore size distribution. It provides a more comprehensive representation of soil-water interactions and is applicable to a wide range of soil types across the entire suction range. The FX model, similar to the VG model, was developed by modifying the pore size distribution function proposed by van Genuchten MT (1980). Due to its validity and simplicity, this study adopts the van Genuchten model to simulate the experimental data. The van Genuchten model is expressed as follows (Equ. 1).

$$\theta = \theta_r + \frac{(\theta_s - \theta_r)}{[1 + (a \cdot s)^n]^m} \quad (1)$$

where θ_r and θ_s are residual and saturated volumetric water content, respectively, which can be accessed from SWCC data. a, n and m are model parameters, which are related to

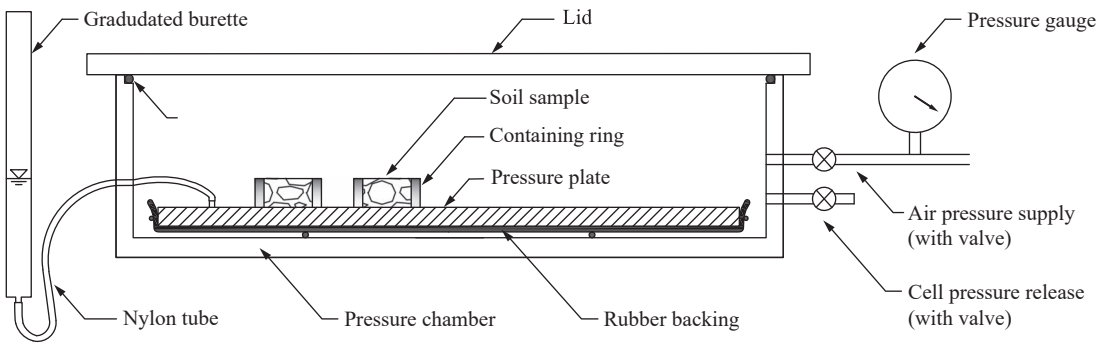

Fig. 6. Schematics of the pressure plate apparatus.

the inverse of air entry value, pore size distribution of soil and the overall symmetry of the soil water characteristic curve, respectively. These parameters can be determined by fitting the SWCC experimental data.

Another important parameter related to hydraulic properties is hydraulic conductivity, often referred to as the permeability coefficient, which reflects the ease of water migration in the soil. Hydraulic conductivity can be applied to many engineering disciplines, such as settlement determination for landslides or foundation caused by moisture infiltration, irrigation and drainage system design, and environmental risk assessment (Gribb MM et al., 2004; Wang Y et al.,2013; Yao RJ et al., 2015; Lu Y et al., 2021). For unsaturated soils, the directly determining measurements for hydraulic conductivity are often laborious, time-consuming, and not cost-effective (Saxton KE and Rawls WJ, 2006). Moreover, the unsaturated hydraulic conductivity is not a fixed value; instead, it varies depending on the water content and pore size distribution, which adds complexity to the situation. Fortunately, this variability can be accurately described using statistical models based on SWCC. The VG model has shown excellent performance in determining SWCC, leading to wide acceptance of the hydraulic conductivity expressions derived from it. The equation based on the van Genuchten-Mualem function (Mualem Y, 1976; van Genuchten MT, 1980) is provided as a reliable approach (Equs. 2, 3).

$$k_r = k_s S_e^l \left(1 - \left(1 - (S_e)^{\frac{1}{m}}\right)^m\right)^2 \tag{2}$$

$$S_e = \frac{\theta - \theta_r}{\theta_s - \theta_r} \tag{3}$$

where k_r is the unsaturated hydraulic conductivity, k_s is the saturated hydraulic conductivity, S_e is the effective saturation, and l is a model parameter which can be determined by regression of the SWCC and a value of 0.5 is frequently taken. To utilize this equation, it is imperative to possess knowledge of the saturated hydraulic conductivity of the soil. The determination of the saturated hydraulic conductivity can be achieved experimentally by employing Darcy's law, which is expressed as (Equ. 4):

$$v = k_s i \tag{4}$$

where v is the seepage velocity, k_s is the saturated hydraulic conductivity, and i is the hydraulic gradient, defined as the ratio of the head difference between the two points to the seepage length between the two points, i.e. $i=H/L$, when seepage occurs between any two points in the soil. According to this formula, the saturated permeability coefficient of the soil sample can be back calculated by measuring the velocity of water flowing through the soil sample and the hydraulic gradient in the process.

Within this investigation, the variable head penetration test is conducted utilizing the TST-55 permeameter. The schematic diagram is shown in the Fig. 7. Before commencing the test, it is essential to flush the equipment with water to ensure the removal of any air bubbles within the pipes. Subsequently, the saturated soil sample is securely placed in a sample container. A constant flow of water from the water reservoir should be directed towards the soil sample until a steady outflow of water is observed from the drainage pipe. At this juncture, the valve connected to the water reservoir should be closed, and the penetration of the soil sample should be initiated using the water within the variable head tube. It is necessary to accurately record the initial water head at the commencement of the experiment and simultaneously begin timing. After a predetermined period of time, the current water head value should be recorded, at which point the timing should be halted, effectively concluding the experiment.

During the experiment, since the water head gradually changes with time, assuming that after dt time, the water level in the variable head pipe decreases by dh, then the amount of water flowing through the soil sample during dt time can be expressed as (Equ. 5):

$$dq_1 = -adh \tag{5}$$

where the negative sign indicates that the water volume increases as dh decreases. According to Darcy's Law, the amount of water seeping out of the sample within dt time is (Equ. 6):

$$dq_2 = kiAdt = k\frac{\Delta H}{L}Adt \tag{6}$$

When the soil sample is completely saturated, the quantity of water descending within the variable head pipe should equate to the amount of water passing through the soil sample,

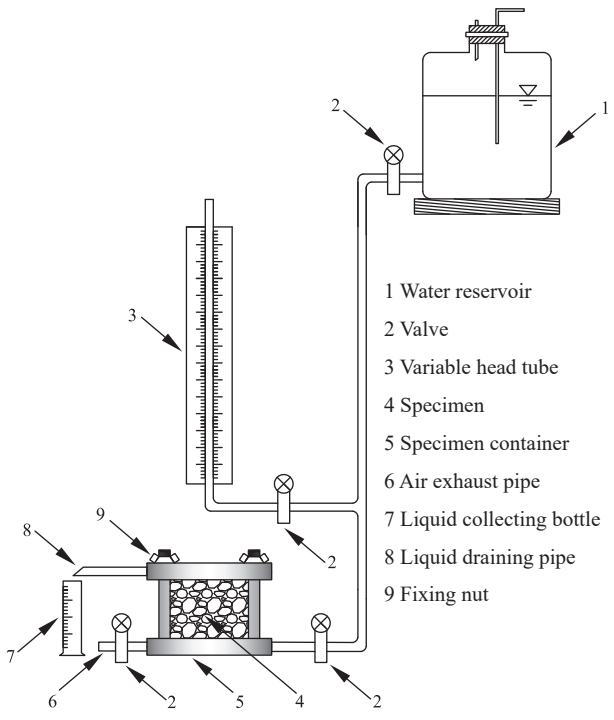

Fig. 7. Schematic of test setup of variable head penetration test.

denoted as $dq_1 = dq_2$. Combining the aforementioned equations and conducting integration will yield the expression for the permeability coefficient.

$$k_s = 2.3\frac{aL}{A(t_2 - t_1)}lg\frac{H_1}{H_2} \quad (7)$$

Where a is the cross-sectional area of the variable water head pipe, L is the penetration path, that is, the height of the sample, A is the cross-sectional area of the sample, t_1, t_2 are the starting and ending times of measuring the water head, and H_1, H_2 are the starting and ending water heads.

5. Results

5.1. SWCC test results

The results of the pressure plate test are listed in Table 2, which are then plotted and presented in the Fig. 8. Distinct differences in the water retention capacity of soil samples obtained from these three locations can be observed. TS loess exhibits the highest SWCC distribution position, followed by DX loess, with LZ loess displaying the lowest position. Thus, it can be inferred that under equivalent matric suction conditions, the ability of soil samples to retain moisture from highest to lowest is as follows: TS loess, DX loess, and LZ loess. Furthermore, it should be noted that among the three soil samples, TS loess also demonstrates the highest saturated moisture content and residual moisture content. This indicates that, as a whole, TS loess possesses a superior water retention capacity.

To determine the mathematical expression of SWCC for each soil sample thereby enabling continuous prediction of changes in water retention capacity, the van Genuchten model was utilized to fit the experimental data. The fitting results are shown in Fig. 9. It is evident that the VG model captures the SWCC data of all three samples, adequately depicting the variations in water retention capacity with minimal deviation. The corresponding parameters used for the fitting process are provided in the Table 3.

5.2. Hydraulic conductivity test results

The saturated hydraulic conductivity test results obtained via variable head penetration test are 1.02 mm/min for Lanzhou Loess, 0.89 mm/min for Tianshui Loess, and 0.94 mm/min for Dingxi loess, respectively. For a more intuitive comparison, the experimental results are depicted in Fig. 10. The figure demonstrates that among the tested loess samples, Lanzhou loess exhibits the highest saturated hydraulic conductivity, followed by Dingxi loess, while Tianshui loess displays the lowest hydraulic conductivity. The hydraulic conductivity serves as a comprehensive indicator of various factors, including the size of soil voids, the compactness of the soil structure, and the content of clay minerals. The observation that Lanzhou loess possesses a larger permeability coefficient aligns well with the results obtained from previous tests conducted, such as the particle size distribution (PSD) test and the soil water characteristic curve (SWCC) test.

By utilizing the obtained k_s values, coupled with the SWCC attained in this study and its corresponding fitting parameters, the unsaturated hydraulic conductivity can now be predicted, as presented in Fig. 11.

5.3. Microstructural observation

To gain a comprehensive and profound understanding, SEM observations were conducted on Lanzhou, Tianshui and Dingxi samples, and the observed findings are displayed in Fig. 12. In the provided figure, it is evident that the loess soil particles in Lanzhou exhibit distinct outlines, with noticeable unfilled gaps between them. Conversely, the soil particles of Tianshui loess present a less pronounced outer outline, and the gaps between particles are filled with smaller particles, resulting in a more continuous and denser state overall. This observation suggests a higher concentration of clay minerals and cements within the soil. As for the loess found in Dingxi, its particle structure lies somewhere between the two. This means that clear outer contours of the particles as well as the gaps filled with smaller particles can be observed, along with the presence of cement.

6. Discussion

The influence and mechanism of water retention performance on landslide stability can be elucidated from various perspectives. Firstly, loess exhibits unique structural characteristics. When the soil has low water content, it possesses good strength due to the presence of cement from crystallized salts and matric suction. However, upon contact with water, the cement dissolves and the matric suction dissipates, leading to a rapid loss of soil strength and creating potential landslide hazards. The water retention capacity of the soil plays a crucial role in this phenomenon. A soil with robust water retention capacity will retain water for a longer duration under similar conditions, impeding the generation of aforementioned cement and matric suction. Consequently, a

Table 2. SWCC test data of LZ, TS and DX loess samples.

Soil sample	Suction Level/kPa														
	0	10	20	50	100	150	200	300	400	500	600	700	900	1200	1400
	Volumetric Water Content														
LZ Loess	0.45	0.40	0.35	0.22	0.17	0.15	0.13	0.10	0.10	0.09	N.A.	0.09	0.09	0.08	0.08
TS Loess	0.53	0.45	0.39	0.28	0.24	0.22	0.21	0.20	0.19	0.18	0.18	0.17	0.17	0.16	0.16
DX Loess	0.49	0.44	0.37	0.26	0.22	0.20	0.18	0.16	0.16	0.15	N.A.	0.14	0.13	0.13	0.12

high water retention capacity results in the loess maintaining a weaker state for an extended period, which is detrimental to the stability of loess landslides.

Secondly, the moisture content in the soil contributes to an increased self-weight of the soil. In other words, it will increase the disturbance force of landslides, which is also very detrimental to landslide stability. Soil with enhanced water retention capacity will hold moisture in the soil for a prolonged period, thereby impacting landslide stability. In summary, the soil's water-holding capacity affects both the resistive and disturbing forces of landslides, playing a pivotal role in landslide stability.

Moreover, water in the soil possesses a lubricating effect, diminishing the frictional resistance and facilitating the rearrangement of soil particles and rendering the soil more susceptible to deformation, posing a threat to landslide stability. A soil with heightened water retention capacity will prolong the soil's deformable state, further compromising the stability of landslides. To make matters worse, the ubiquitous presence of mudstone beneath the loess layer exacerbates the situation by creating conditions conducive to water accumulation near the contact interface, potentially resulting in soil saturation. During this critical phase, if external forces, such as seismic effects, come into play, the landslide body

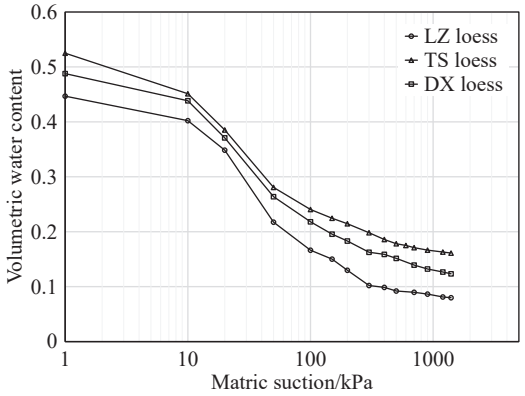

Fig. 8. SWCC data of LZ, TS and DX loess samples.

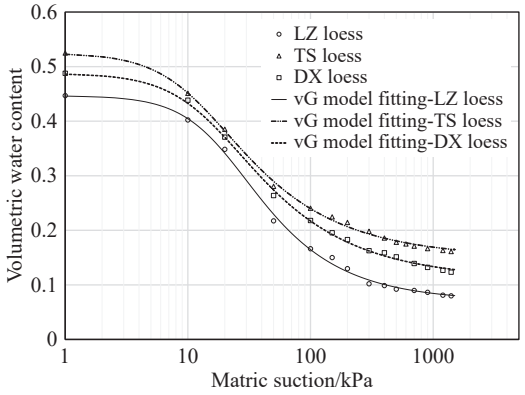

Fig. 9. SWCC fitting curves by using VG model for LZ, TS and DX loess samples.

Table 3. Fitting parameters used by VG model for LZ, TS and DX loess samples.

Sample	Model Parameters			R^2	RMSE
	a	*n*	*m*		
LZ Loess	0.05176	1.827	0.4527	0.9979	0.006
TS Loess	0.08207	1.673	0.4023	0.9984	0.0049
DX Loess	0.06468	1.666	0.3998	0.9985	0.0048

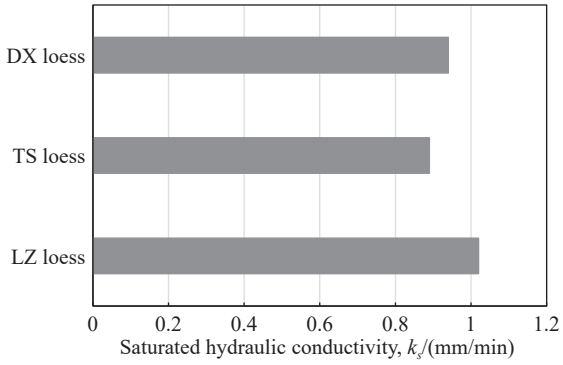

Fig. 10. Saturated hydraulic conductivity for LZ, TS and DX loess samples.

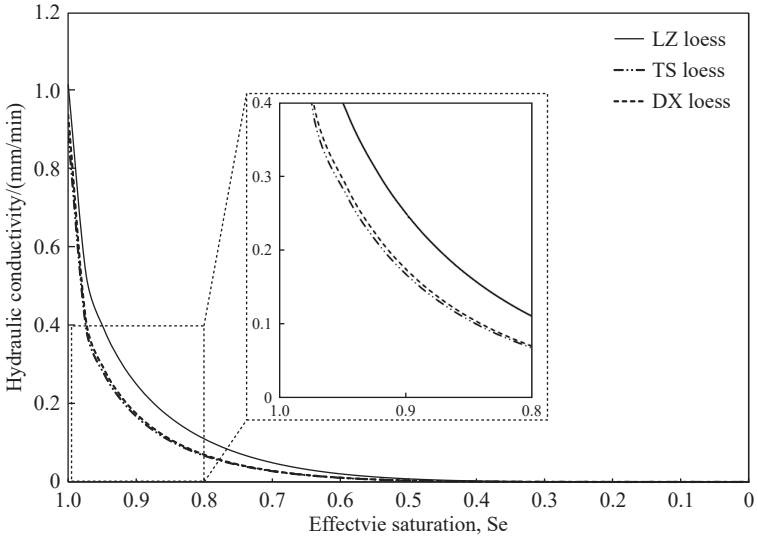

Fig. 11. Predicted hydraulic conductivity for LZ, TS and DX loess samples.

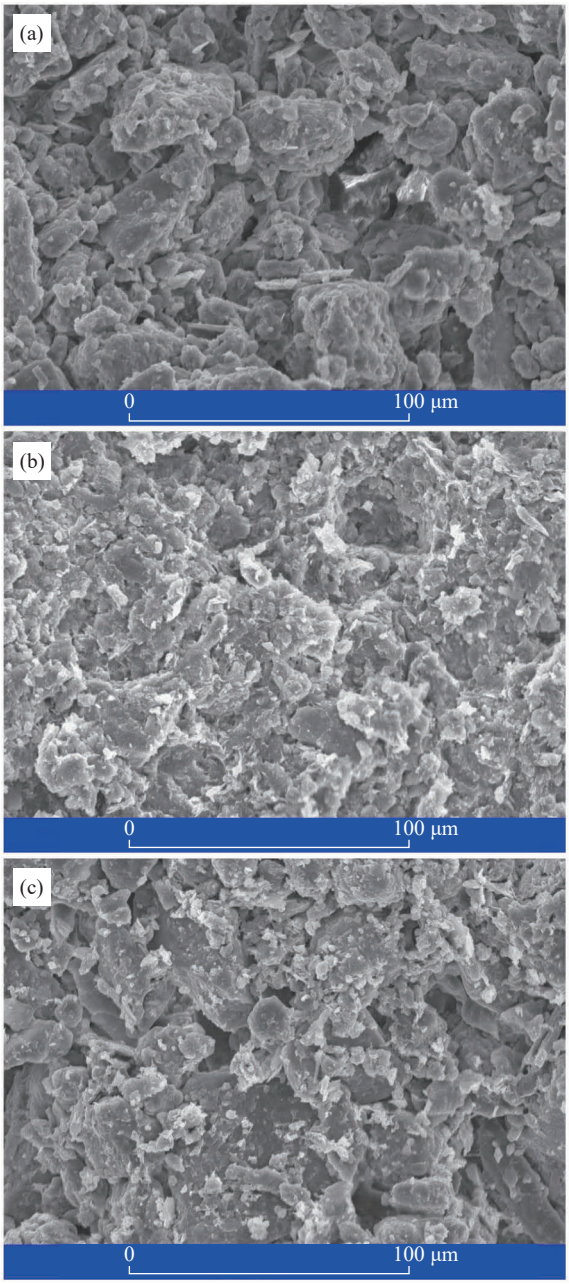

Fig. 12. SEM images of for LZ, TS and DX loess samples. a–Lanzhou loess, b–Tianshui loess, and c–Dingxi loess.

becomes even more susceptible to instability and failure.

On the whole, the stronger water holding capacity enables prolonged moisture retention within the soil, thereby extending the duration of the aforementioned unfavorable conditions and posing threats to the stability of landslides. Upon observing the Fig. 1, a higher occurrence of landslide disasters in the Weihe River system between Tianshui and Dingxi is found, compared to the Yellow River system around Lanzhou and Dingxi. The experimental results of this study, along with the corresponding theoretical analysis, provide a rational explanation for this observation.

Regarding the hydraulic conductivity, it is worth noting that a lower hydraulic conductivity generally indicates a greater difficulty for surface water to penetrate deeply into the soil. This condition proves beneficial for maintaining the stability of landslides. However, due to the unique characteristics of loess, vertical joints within the soil are extensively developed, making it a favorable pathway for surface water to rapidly migrate into the deeper layers of the soil. When water accumulates at the interface of mudstone and saturates loess, the dissipation of water within the loess becomes closely dependent on its permeability coefficient. During this stage, a lower permeability coefficient impedes water drainage instead. Consequently, the Tianshui loess, known for its high water retention capacity and low permeability, can impose a greater threat to the stability of landslides.

Observations of the microstructure indicate that among the three soil samples examined, Lanzhou loess possesses the highest porosity and the least density, Tianshui loess is characterized by the greatest density, and Dingxi loess displays intermediate properties. Smaller voids and a denser structure are associated with increased water retention capacity and decreased permeability. The microstructure observations from the SEM test align well with the findings from the previous SWCC experiment and permeability coefficient experiment. These experimental results mutually support each other, resulting in significant progress.

7. Conclusion

This study focused on the hydraulic behaviors of loess in landslide-prone areas of the Loess Plateau, providing insights into the regional landslide hazards by examining samples from Lanzhou, Dingxi, and Tianshui —densely-inhabited cities with frequent landslides. By comparing water retention capacity and permeability through soil water characteristic curves (SWCC) tests and saturated hydraulic conductivity tests, and integrating them into the van Genuchten model, a clear trend emerged: Tianshui loess processes greater water-holding capacity and lower permeability than in Dingxi and Lanzhou, indicating a higher susceptivity to landslides. Scanning Electron Microscope (SEM) analyses showed that Lanzhou loess had more macropores leading to greater permeability, whereas the Tianshui loess was denser, with Dingxi loess falling in between. This microstructural evidence corroborated the SWCC and permeability results, lending further validation to the findings. The study's outcomes reveal the critical nature of loess properties in relation to landslide risks and emphasize the necessity of considering these factors in hazard prevention and engineering practices, contributing to more comprehensive macroscopic analyses of landslide hazards in loess regions.

CRediT authorship contribution statement

Gao-chao Lin, Wei Liu and Xing Su conceived of the presented idea. Gao-chao Lin proposed the research framework, Wei Liu and Xing Su carried out the experiment. All authors discussed the results and contributed to the final manuscript.

Declaration of competing interest

The authors declare no conflicts of interest.

Acknowledgment

The authors are grateful for the financial support for the research presented in this paper from National Natural Science Foundation of China (42201142, 42067066, 51778590).

References

Brooks R, Corey A. 1964. Hydraulic properties of porous media. Hydrology Paper No. 3, Colorado State University, Fort Collins, CO.

Chen WW, Liu W, Wu WJ, Ye F, Su X, Xu H. 2016. Study on the characteristics and origin of Huanancun Landslide. Journal of Engineering Geology, 24, 533–539. doi: 10.13544/j.cnki.jeg.2016.s1.077.

Chen JC, Wang LM, Wang P, Che AL. 2022. Failure mechanism investigation on loess–mudstone landslides based on the Hilbert–Huang transform method using a large-scale shaking table test. Engineering Geology, 302, 106630. doi: 10.1016/j.enggeo.2022.106630.

Cheng YX, Zhang J, Du DJ. 2007. On the relationship between fault and activity and geological hazard in Tianshui area, Gansu province. Journal of Engineering Geology, 15(1), 33–37.

Derbyshire E, Meng XM, Dijkstra TA. 2000. Landslides in the thick loess terrain of North-West China. Wiley, Hoboken, 1–288. doi: 10.1046/j.1365-2451.2002.03438.x.

Derbyshire E. 2001. Geological hazards in loess terrain, with particular reference to the loess regions of China. Earth Science Review, 54, 231–260. doi: 10.1016/S0012-8252(01)00050-2.

Fredlund DG, Xing A. 1994. Equations for the soil-water characteristic curve. Canadian Geotechnical Journal, 31(4), 521–532. doi: 10.1139/t94-061.

Gribb MM, Kodesova R, Ordway SE. 2004. Comparison of soil hydraulic property measurement methods. Journal of Geotechnical and Geoenvironmental Engineering, 130, 1084–1095. doi: 10.1061/(asce)1090- 0241(2004)130:10(1084).

Guo FY, Meng XM, Li ZH. 2015. Characteristics and causes of assembled geo-hazards induced by the rainstorm on 25th July 2013 in Tianshui city, Gansu, China. Mountain Research, 33(1), 100–107.

Hu HJ. 2018. Study on the method for determining the unsaturated permeability coefficient of loess in humidification. Journal of Hydraulic Engineering, 49(10), 1216–1226.

Huang QB, Jia XN, Peng JB, Liu Y, Wang T, 2019. Seismic response of loess-mudstone slope with bedding fault zone. Soil Dynamics and Earthquake Engineering Journal, 123, 371–380. doi: 10.1016/j.soildyn.2019.05.009.

Jia XN, Huang QB. , Peng JB, Lan HX, Liu Y. 2022. Seismic response of loess-mudstone slope with high anti-dip angle fault zone. Applied Sciences, 12(13), 6353. doi: 10.3390/app12136353.

Jiao X, Liu G, Tu X. 2014. Estimat on of water resources carrying capacity for revegetation in the Loess Plateau. Journal of Hydraulic Engineering, 45, 1344–1351.

Khanal A, Klavon KR, Fox GA, Daly ER. 2016. Comparison of linear and nonlinear models for cohesive sediment detachment: Rill erosion, hole erosion test, and streambank erosion studies. Journal of Hydraulic Engineering, 142(9), 04016026. doi: 10.1061/(ASCE)HY.1943-7900.0001147.

Li TL, Long JH, Li XS. 2007. Types of loess landslides and methods for their movement forecast. Journal of Engineering Geology, 15(4), 500–505.

Li YR, Mo P. 2019. A unified landslide classification system for loess slopes: A critical review. Geomorphology, 340, 67–83. doi: 10.1016/j.geomorph.2019.04.020.

Liang CY, Zhang H, Wang T. 2022. Red clay/mudstone distribution, properties and loess–mudstone landslides in the Loess Plateau, China. Environ. Earth Science, 81, 386. doi: 10.1007/s12665-022-10489-4.

Lin GC, Liu W, Zhao JX, Fu PC. 2023. Experimental investigation into effects of lignin on sandy loess. Soils Foundation, 63, 101359. doi: 10.1016/j.sandf.2023.101359.

Lin ML, Wang KL. 2006. Seismic slope behavior in a large-scale shaking table model test. Engineering Geology, 86(2), 118–133. doi: 10.1016/j.enggeo.2006.02.011.

Liu TS, Wang TM, Wang KL, Wen CC. 1964. Loess on the middle reaches of the Yellow River. Beijing, Science Press, 234 (in Chinese).

Liu TS. 1985. Loess and The Environment. Beijing, China Ocean Press, 1–237 (in Chinese).

Liu W, Lin GC, Su X. 2023. Effects of pre-dynamic loading on hydraulic properties and microstructure of undisturbed loess. Journal of Hydrology, 622, 129690. doi: 10.1016/j.jhydrol.2023.129690.

Liu FY, Zhang Z. 2008. Study on effect of infiltration paths on water-air permeability coefficients in unsaturated loess. Journal of Hydraulic Engineering, 39(8), 934–939.

Lu Y, Liu S, Zhang Y, Wang L, Li Z. 2021. Hydraulic conductivity of gravelly soils with various coarse particle contents subjected to freeze-thaw cycles. Journal of Hydrology, 598, 126302. doi: 10.1016/j.jhydrol.2021.126302.

Metelková Z, Boháč J, Přikryl R. 2012. Maturation of loess treated with variable lime admixture: pore space textural evolution and related phase changes. Applied Clay Science, 61, 37–43. doi: 10.1016/j.clay.2012.03.008.

Mu P, Wu WJ, Wang SC. 2010. An analysis of treatment effect for the Shixiakou Landslide in Lanzhou. Hydrogeology and Engineering Geology, 37(4), 87–91 (in Chinese with English).

Mualem Y. 1976. A new model for predicting the hydraulic conductivity of unsaturated porous media. Water Resource Research, 12, 513–522. doi: 10.1029/WR012i003p00513.

Saxton KE, Rawls WJ. 2006. Soil water characteristic estimates by texture and organic matter for hydrologic solutions. Soil Science Society of America Journal, 70, 1569–1578. doi: 10.2136/sssaj2005.0117.

Srilatha N, Latha GM, Puttappa CG. 2013. Effect of frequency on seismic response of reinforced soil slopes in shaking table tests. Geotextiles and Geomembranes, 36(1), 27–32. doi: 10.1016/j.geotexmem.2012.10.004.

Taylor SR, McLennan SM, McCullouch MT. 1983. Geochemistry of loess, continental crustal composition and crustal model ages. Geochimica et Cosmochimica Acta, 47(11), 1897–1905. doi: 10.1016/0016-7037(83)90206-5.

van Genuchten MT. 1980. A closed-form equation for predicting the hydraulic conductivity of unsaturated soils. Soil Science Society of America Journal, 44(5), 892–898. doi: 10.2136/sssaj1980.03615995004400050002x.

Wang SQ, Unwin DJ. 1992. Modelling landslide distribution on loess soils in China: An investigation. International Journal of Geographical Information Systems, 6(5), 391–405. doi: 10.1080/02693799208901922.

Wang KL, Lin ML. 2011. Initiation and displacement of landslide induced by earthquake - a study of shaking table model slope test. Engineering Geology, 122(1–2), 106–114. doi: 10.1016/j.enggeo.2011.04.008.

Wang Y, Shao MA, Liu Z, Horton R. 2013. Regional-scale variation and

distribution patterns of soil saturated hydraulic conductivities in surface and subsurface layers in the loessial soils of China. Journal of Hydrology, 487, 13–23. doi: 10.1016/j.jhydrol.2013.02.006.

Wang HJ, Sun P, Han S. 2020. Failure mechanism of the Changhe Landslide on september 14, 2019 in Tongwei, Gansu. Geoscience, 35(3), 732–743. doi: 10.19657/j.geoscience.1000-8527.2020.073.

Wang XG, Lian BQ, Liu K, Luo L. 2021. Trigger mechanism of loess-mudstone landslides inferred from ring shear tests and numerical simulation. Journal of Mountain Science, 18(9), 2412–2426. doi: 10.1007/s11629-021-6791-6.

Wang H, Li TL, Fu YK. 2014. Determining permeability function of unsaturated loess by using instantaneous profile method. Journal of Hydraulic Engineering, 45(8), 997–1003.

Wang X, Zhou YH, Wang YK, Wei X, Guo X, Zhu D. 2015. Soil water characteristic of a dense jujube plantation in the semi-arid hilly Regions of the Loess Plateau in China. Journal of Hydraulic Engineering, 46(3), 263–270. doi: 10.13243/j.cnki.slxb.2015.03.002.

Walder JS. 2016. Dimensionless erosion laws for cohesive sediment. Journal of Hydraulic Engineering, 142(2), 04015047. doi: 10.1061/(ASCE)HY.1943-7900.000106.

Wen BP, Lei H. 2012. Influence of lixiviation by irrigation water on residual shear strength of weathered red mudstone in Northwest China: Implication for its role in landslides' reactivation. Engineering Geology, 151, 56–63. doi: 10.1016/j.enggeo.2012.08.005.

Wu WJ, Wang NQ. 2002. Basic types and active features of loess landslide. The Chinese Journal of Geological Hazard and Control, 13(2), 36–40.

Wu WJ. 2003. Landslide and debris flow hazards in City of Tianshui. Hydrogeology and Hydrologic Engineering, 30(5), 75–78.

Wu WJ, Wang DK, Su X. 2008. Basic types and active characteristics of loess landslide in China. Landslides and engineering slopes. London, Taylor and Francis Group, 519–524.

Xin ZX, Han QX. 1988. Distribution characteristics and macroscopic mechanism of landslides in the Loess Plateau. Soil and Water Conservation in China, 6, 21–25. doi: 10.14123/j.cnki.swcc.1988.06.006.

Xin CL, Yang GL, Zhao ZP. 2012. Geo-hazard types and causes analysis in Tianshuishi Beishan. The Chinese Journal of Geological Hazard and Control, 23(2), 89–95.

Xu L, Dai FC, Kwong AKL. 2008. Types and characteristics of loess landslides at Heifangtai Loess Plateau. Journal of Mountain Science, 26(3), 364–371.

Xu L, Dai FC, Min H. 2010. Loess landslide types and topographic features at South Jingyang Plateau, China Earth Sciences, 35(1), 155–160. doi: 10.1144/qjegh2018-115.

Xu L, Coop MR, Zhang M, Wang GL. 2018. The mechanics of a saturated silty loess and implications for landslides. Engineering Geology, 236, 29–42. doi: 10.1016/j.enggeo.2017.02.021.

Xu YR, Allen MB, Zhang WH, Li WQ, He HL. 2020. Landslide characteristics in the Loess Plateau, northern China. Geomorphology, 359, 107150. doi: 10.1016/j.geomorph.2020.107150.

Yao RJ, Yang JS, Wu DH, Li FR, Gao P, Wang XP. 2015. Evaluation of pedo-transfer functions for estimating saturated hydraulic conductivity in coastal salt-affectedmud farmland. Journal of Soils Sediments, 15, 902–916. doi: 10.1007/s11368-014-1055-5.

Yu TF, Huang QB, Kang XS, Liu X, Xie QY. 2023. On seismic response of loess-mudstone slope with underlying anti-dip fault zone: laboratory investigation using shaking table test. Bulletin of Engineering Geology and the Environment, 82, 117. doi: 10.1007/s10064-023-03158-8.

Zhang ZL, Wang T, Wu SR, Tang HM, Liang CY. 2017. Seismic performance of loess-mudstone slope in Tianshui – Centrifuge model tests and numerical analysis. Engineering Geology, 222, 225–235. doi: 10.1016/j.enggeo.2017.04.006.

Zhang S, Xu Q, Hu ZM. 2016. Effects of rainwater softening on red mudstone of deep-seated landslide, Southwest China. Engineering Geology, 204, 1–13. doi: 10.1016/j.enggeo.2016.01.013.

Zhang CL, Li P, Li TL, Zhang MS. 2014. In-situ observation on rainfall infiltration in loess. Journal of Hydraulic Engineering, 45(6), 728–734. doi: 10.13243/j.cnki.slxb.2014.06.012.

Zhang ZL, Zeng RQ, Meng XM, Zhao SF, Ma JH, Wang H, Meng XP, Yin HL, Yao YQ, Guo WW, Xie DJ, He B. 2022. Effects of material migration on the spatial distribution of topsoil moisture at the slope scale. Engineering Geology, 308, 106820. doi: 10.1016/j.enggeo.2022.106820.

Zhang ZL, Zeng RQ, Meng XM, Zhao SF, Wang SX, Ma JH, Wang H. 2023. Effects of changes in soil properties caused by progressive infiltration of rainwater on rainfall-induced landslides. Catena, 233, 107475. doi: 10.1016/j.catena.2023.107475.